

Locating the intense interstellar scattering towards the inner Galaxy

J. Dexter^{1,2*}, A. Deller^{3,4}, G.C. Bower⁵, P. Demorest⁶, M. Kramer^{7,8},
B.W. Stappers⁸, A.G. Lyne⁸, M. Kerr⁹, L.G. Spitler⁷, D. Psaltis^{10,11},
M. Johnson¹², R. Narayan¹²

¹Max Planck Institute for Extraterrestrial Physics, Giessenbachstr. 1, 85748 Garching, Germany

²Kavli Institute for Theoretical Physics, University of California, Santa Barbara, CA 93106, USA

³ASTRON, the Netherlands Institute for Radio Astronomy, Postbus 2, 7990 AA, Dwingeloo, The Netherlands

⁴Centre for Astrophysics and Supercomputing, Swinburne University of Technology, PO Box 218, Hawthorn, VIC 3122, Australia

⁵Academia Sinica Institute of Astronomy and Astrophysics, 645 N. A'ohoku Place, Hilo, HI 96720, USA

⁶National Radio Astronomy Observatory, Socorro, New Mexico 87801, USA

⁷Max Planck Institute for Radio Astronomy, Auf dem Hügel 69, 53121, Bonn Germany

⁸Jodrell Bank Centre for Astrophysics, University of Manchester, Manchester, M13 9PL, UK

⁹Space Science Division, Naval Research Laboratory, Washington, DC 20375-5352, USA

¹⁰University of Arizona, 933 N. Cherry Ave, Tucson, AZ 85721, USA

¹¹Radcliffe Institute for Advanced Study and Black-Hole Initiative, Harvard University, 10 Garden St., Cambridge, MA 02138

¹²Harvard-Smithsonian Center for Astrophysics, 60 Garden Street, Cambridge, MA 02138, USA

Accepted XXX. Received YYY; in original form ZZZ

ABSTRACT

We use VLBA+VLA observations to measure the sizes of the scatter-broadened images of 6 of the most heavily scattered known pulsars: 3 within the Galactic Centre (GC) and 3 elsewhere in the inner Galactic plane ($\Delta l < 20^\circ$). By combining the measured sizes with temporal pulse broadening data from the literature and using the thin-screen approximation, we locate the scattering medium along the line of sight to these 6 pulsars. At least two scattering screens are needed to explain the observations of the GC sample. We show that the screen inferred by previous observations of SGR J1745–2900 and Sgr A*, which must be located far from the GC, falls off in strength on scales $\lesssim 0.2$ degree. A second scattering component closer to ($\Delta < 2$ kpc) or even (tentatively) within ($\Delta < 700$ pc) the GC produces most or all of the temporal broadening observed in the other GC pulsars. Outside the GC, the scattering locations for all three pulsars are $\simeq 2$ kpc from Earth, consistent with the distance of the Carina-Sagittarius or Scutum spiral arm. For each object the 3D scattering origin coincides with a known HII region (and in one case also a supernova remnant), suggesting that such objects preferentially cause the intense interstellar scattering seen towards the Galactic plane. We show that the HII regions should contribute $\gtrsim 25\%$ of the total dispersion measure (DM) towards these pulsars, and calculate reduced DM distances. Those distances for other pulsars lying behind HII regions may be similarly overestimated.

Key words: Galaxy: centre — pulsars: general — scattering — HII regions — ISM: supernova remnants

1 INTRODUCTION

Interstellar scattering from electron density inhomogeneities leads to multipath propagation, broadening the radio images and pulse profiles of objects in or behind the Galactic

plane. Along certain lines of sight, the scattering is “intense” – much larger than predicted by the large-scale components of the Galactic electron distribution (Taylor & Cordes 1993; Cordes & Lazio 2002). It has long been associated with HII regions and/or supernova remnants near the line of sight (e.g., Litvak 1971; Little 1973; Demison et al. 1984).

* E-mail: jdexter@mpe.mpg.de

The Galactic Centre black hole, Sgr A*, provides a

well known example of intense scattering. Its image size increases as λ^2 in the radio (e.g., [Davies et al. 1976](#); [Backer 1978](#); [Bower et al. 2006](#)) as predicted for a “thin” scattering medium (e.g., [Ishimaru 1977](#); [Blandford & Narayan 1985](#)). The large angular size of Sgr A* was previously thought to come from the hot, dense gas in the Galactic Centre (GC) region. Producing the large observed image close to the source would require a special scattering geometry ([Goldreich & Sridhar 2006](#)). It would also prevent the detection of pulsed radio emission from neutron stars in the GC, potentially explaining the lack of pulsar detections in the central parsec of the Galaxy ([Cordes & Lazio 1997](#); [Lazio & Cordes 1998](#)).

Radio pulsations discovered from the GC magnetar SGR J1745–2900 ([Eatough et al. 2013](#)), only 0.1 pc in projection from Sgr A*, were broadened by orders of magnitude less than predicted ([Spitler et al. 2014](#)). In addition, the image size and shape of the magnetar match that of Sgr A*, showing that they share the same scattering medium ([Bower et al. 2014](#)). The scattering medium towards Sgr A* therefore does not prevent the detection of ordinary pulsars at frequencies $\gtrsim 3$ GHz. The known young stars in the central parsec imply a large population of young pulsars. Assuming that the magnetar scattering medium is representative of the central parsec, the stated sensitivities of deep radio searches to date and the lack of detections suggest a “missing pulsar problem” in the central parsec ([Johnston 1994](#), [Macquart et al. 2010](#), [Dexter & O’Leary 2014](#); but see also [Chennamangalam & Lorimer 2014](#); [Rajwade et al. 2016](#); [Psaltis et al. 2016](#)).

Combining angular and temporal broadening measures for the same source gives an estimate for the line of sight distance to the scattering medium ([Gwinn et al. 1993](#); [Britton et al. 1998](#)). Using this technique, [Bower et al. \(2014\)](#) showed that the scattering medium towards the magnetar and Sgr A* is not local to the GC, but rather at a distance $\simeq 2 - 3$ kpc from Earth, in the nearby Carina-Sagittarius or Scutum spiral arm. The chance alignment of an ionized gas cloud with Sgr A* is highly unlikely unless such clouds cover a significant fraction of the Galactic plane.

Maser sources are heavily scatter-broadened out to scales of $\simeq 0.5$ degree from Sgr A* ([van Langevelde et al. 1992](#)). Observations of Sgr A* and the magnetar show that the scattering medium extends over scales of arcseconds, but it is not clear how much if any of the rest of the observed scattering in the GC (here defined as the central 0.5 deg) has the same physical origin. The nearest known pulsars to the magnetar are at separations $\simeq 0.2$ degree ([Johnston et al. 2006](#); [Deneva et al. 2009](#)). Along with the magnetar, they are the most temporally broadened known pulsars (e.g., [Manchester et al. 2005](#)).

To study the GC screen and the physical origin of intense scattering, we imaged a sample of strongly scattered pulsars (3 GC, 3 non-GC) with VLBA and VLBA+VLA observations (§2). We measure angular broadening from scattering (§3) in all sources that we detected (one source was not detected), and locate the scattering along the line of sight by combining the image sizes with previous temporal broadening measurements (§4). We find evidence for multiple physical locations for the origin of the GC scattering on $\simeq 0.2$ degree scales, and tentative evidence for intense scattering local to the GC. We further show that all three non-

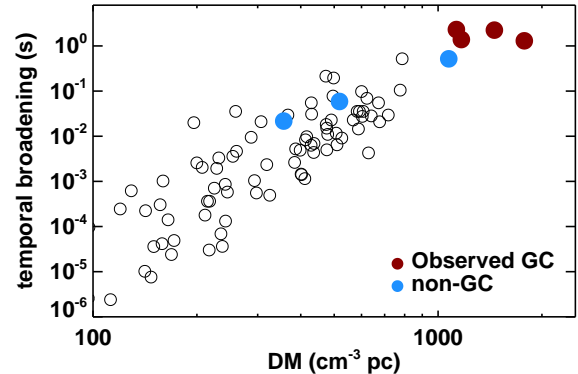


Figure 1. Measured temporal broadening of the pulse profile vs. dispersion measure for known pulsars with high DM and measured τ in the ATNF database ([Manchester et al. 2005](#)). We selected accessible objects with the highest possible DM and τ . The largest τ pulsars all reside within the GC (red points), including the GC magnetar SGR J1745–2900, imaged previously by [Bower et al. \(2014\)](#).

GC sources have scattering origins at distances $\simeq 2 - 3$ kpc from Earth like the GC magnetar and Sgr A*. In all three cases the 3D scattering location coincides with a known HII region, adding to the evidence that such regions may be the dominant cause of intense interstellar scattering in the Galactic plane.

2 OBSERVATIONS AND DATA REDUCTION

2.1 Sample selection

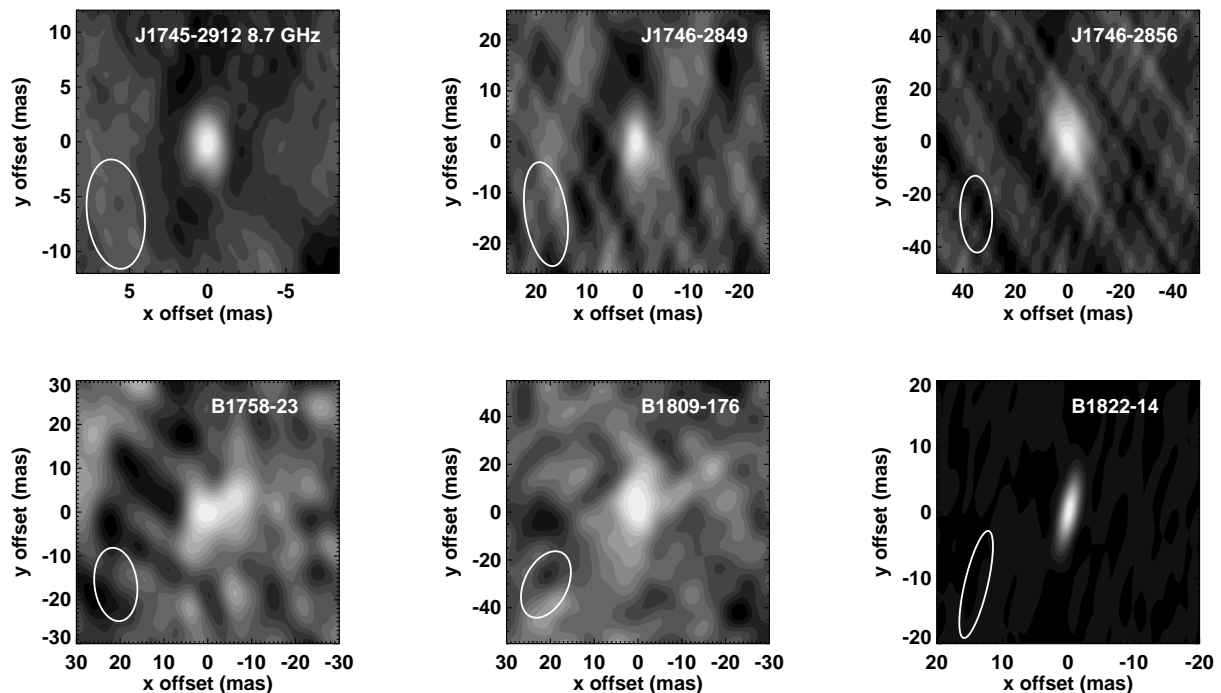
Our sample was chosen to focus on highly scattered pulsars (dispersion measure $DM > 200$ pc cm $^{-3}$, temporal broadening $\tau > 10$ ms at 1 GHz, which were sufficiently bright for imaging with the VLBA only (non-GC sources) or the VLBA+VLA (GC sources).

The sources observed are shown in Figure 1 in the τ -DM plane and further properties are listed in Table 1. The four pulsars with the highest measured τ are all $\lesssim 0.2$ deg from Sgr A* in the GC ([Johnston et al. 2006](#); [Deneva et al. 2009](#); [Eatough et al. 2013](#)). The angular size of the GC magnetar, SGR J1745–2900, was measured by [Bower et al. \(2014\)](#). We observed the 3 other sufficiently bright known GC pulsars. The flat spectrum, young pulsar J1746-2850 was not observed, since it has not been detected in recent observations ([Ng et al. 2015](#); [Schnitzeler et al. 2016](#)) and may be a magnetar-like object whose radio emission has since shut off ([Dexter et al. 2017](#)).

Outside of the GC, the four pulsars observed were chosen as those sufficiently bright to be observable with the VLBA alone and with suitable nearby (≤ 3 degrees) calibrators. Most calibrators near the pulsars are heavily scatter-broadened, and it is often necessary to go to $\simeq 3$ degrees away to find one that is detectable on long baselines. The three sources detected (see below) span a range of an order of magnitude in τ and a factor of a few in DM.

Table 1. Some properties of the observed targets and VLBA+VLA observations

Source	J1745–2912	J1745–2912	J1746–2849	J1746–2856	B1750–24	B1758–23	B1809–176	B1822–14
l (deg)	−0.20	−0.20	0.13	0.12	4.27	6.84	12.91	16.81
b (deg)	−0.18	−0.18	−0.04	−0.21	0.51	−0.07	0.39	−1.00
DM (pc cm ^{−3})	1130	1130	1456	1168	672	1073	518	357
P (s)	0.19	0.19	1.48	0.95	0.53	0.42	0.54	0.28
S14 (mJy)	0.5	0.5	0.4	6.5	2.3	2.2	3.3	2.6
Spectral index	−1.7	−1.7	−1.1	−2.7	−1.0	−1.0	−1.7	−1.1
Obs. Date (UT)	2015-11-30	2016-01-30	2015-11-30	2016-01-30	2015-08-25	2015-08-25	2015-12-26	2015-12-26
Obs. Type	VLBA+VLA	VLBA+VLA	VLBA+VLA	VLBA+VLA	VLBA	VLBA	VLBA	VLBA
Calibrator	J1752-3001	J1752-3001	J1752-3001	J1752-3001	J1755-2232	J1755-2232	J1808-1822	J1825-1718
ν (GHz)	8.7	5.9	8.7	5.9	7.5	7.5	4.5	7.5
Int. time (hr)	1.84	1.58	1.52	1.51	1.75	1.82	1.74	1.68
Image rms (μ Jy)	36	170	58	36	140	230	70	110
Beam size (mas)	5.0×1.8	14.9×6.3	10.3×4.1	14.6×6.1	7.3×2.3	8.4×4.9	14.1×5.2	8.4×1.8
Beam PA (deg)	4.0	2.4	8.5	1.7	−4.2	7.2	−10.2	−13.2

**Figure 2.** Scatter-broadened images of the 6 detected pulsars from our VLBA+VLA sample. The color scale is linear with a dynamic range $\simeq 10$. The restoring beam used by CLEAN is shown as the white ellipse, and is influenced both by the array and source properties, since in most cases extended source structure leads to non-detections on long baselines.

2.2 Observations and correlation

The parameters of the observations are listed in Table 1. Observing frequencies were chosen by matching the expected scattering size given the measured temporal broadening and a single scattering screen at 3 kpc from the Sun to the angular resolution of the inner six stations of the VLBA. Generally the two sizes are comparable for $\nu \simeq 4.5 - 8.7$ GHz. At higher frequency the pulsars are fainter, while at lower frequency the calibrators are often significantly scatter-broadened. Pulsar angular sizes significantly smaller or larger than expected would appear as unresolved or would

not be detected. Since we detected 7/8 sources, the choice of observing frequencies does not bias our results. The GC pulsars are faint and had large predicted sizes (implying high frequencies), so that the increased sensitivity of the VLBA+VLA was needed for detection. In all cases, a data rate of 2 Gbps, corresponding to 256 MHz of bandwidth with dual polarization, was used. For observations where the VLA participated, a tied array beam with filterbank data was produced for all scans on the target pulsars.

The data were correlated with an integration time of 2 seconds and a frequency resolution of 0.5 MHz. For the pulsar sources, gating was employed using ephemerides from

timing observations at Jodrell Bank and Parkes to increase the signal-to-noise ratio. These ephemerides were refined using VLA data from the observations themselves where available, as described below. Amplitude scaling was applied to the gated data to yield period-averaged equivalent flux densities for the pulsars, which facilitates comparisons with timing data where the pulsar flux density is usually quoted in this way.

2.3 Data calibration and reduction

Data reduction was performed with AIPS (Greisen 2003), using the ParselTongue python interface (Kettenis et al. 2006). Standard corrections including *a priori* gain calibration based on logged system temperatures, delay and band-pass calibration on a bright fringe finder source, and delay, phase, and amplitude calibration on the phase reference sources were derived. These cumulative corrections were applied to the gated data on the target pulsars, before these data were split and averaged in frequency to a resolution of 32 MHz. These averaged target datasets were written out in UVFITS format, for imaging and further analysis as described below.

2.4 VLA tied-array data processing

At the VLA it is possible to route the summed-array voltage data stream to a local compute cluster for real-time detection, integration, and recording at high time resolution. For our observing sessions in which the VLA participated, we enabled this mode in parallel with VLBI recording in order to obtain simultaneous wide-band timing measurements of the pulsars to use for gating the VLBI correlation. These data were recorded using 1024 MHz total bandwidth, 8-bit voltage quantization, 1024 frequency channels, 0.5 ms time resolution, and summed polarizations. The frequency ranges observed were 8.3 – 9.3 GHz and 5.5 – 6.5 GHz.

Offline processing including folding and time-of-arrival measurement was done using the DSPSR (van Straten & Bailes 2011) and PSRCHIVE (Hotan et al. 2004) software packages; these data were used to determine a short-term timing ephemeris (absolute pulse phase and spin period) that was used to gate the VLBI correlation. We performed an approximate flux calibration by scaling the data assuming system equivalent flux densities for the summed array of 10 Jy and 11.5 Jy, at 9 GHz and 6 GHz respectively. The resulting period-averaged pulsed flux density measurements for all pulsars are presented in the far right column of Table 2. We conservatively assume $\simeq 50\%$ fractional uncertainty on these measurements.

2.5 Source detection

Imaging was performed using DIFMAP (Shepherd et al. 1994), employing natural weighting for maximum sensitivity to resolved sources. Several targets had significant positional uncertainties ($\lesssim 1$ arcsec in dec); we made images minimally covering a region up to $\pm 3\sigma$ in R.A. and dec. After identifying the pulsar position, we shifted the phase center of the visibility data before averaging, to eliminate bandwidth smearing, and then made the small images centered on the

pulsars shown in Figure 2. The lowest significance detections have $\simeq 6\sigma$ (J1746–2849 and B1809–176), due to a combination of low total flux densities ($\sim 0.1 - 1$ mJy) and resolved sources.

2.6 PSR B1750–24

We did not detect PSR B1750–24 in the gated image, despite a predicted flux density and scatter-broadened image size similar to that of PSR B1758–23, which was detected in the same observation, and comparable image rms noise. Either the source is fainter at 7.5 GHz (e.g. because of a break in the spectrum) or it is more scatter-broadened than expected.

2.7 PSR J1745–2912

The GC pulsar J1745–2912 was found to have a small angular size at 8.7 GHz (top right panel of Figure 2), especially interesting since its temporal broadening was found to be larger even than the GC magnetar (Deneva et al. 2009). To test the frequency-dependence of the angular size, we re-observed J1745–2912 at 5.9 GHz in the same observation as J1746–2856.

Unfortunately, the 5.9 GHz data were strongly affected by RFI, which limits their reliability. The folded data from the VLA tied-array beam shows the pulsar signal with $F_\nu \simeq 0.1$ mJy, comparable to the flux density at 8.7 GHz. However, in the gated image the brightest peak is seen several hundred milliarcseconds (many synthesized beams) away from the source position at 8.7 GHz. Moreover, this same peak is seen in the ungated image, and appears to be largely generated by the shortest baseline (VLA to Pie Town), which is likely the most RFI-prone. If this baseline is flagged, no significant source remains in the gated 5.9 GHz image. Accordingly, we make use only of the 8.7 GHz data for this pulsar; however, the failure to detect the pulsar in the 5.9 GHz image given the clear detection of pulsations in the tied-array beam is puzzling.

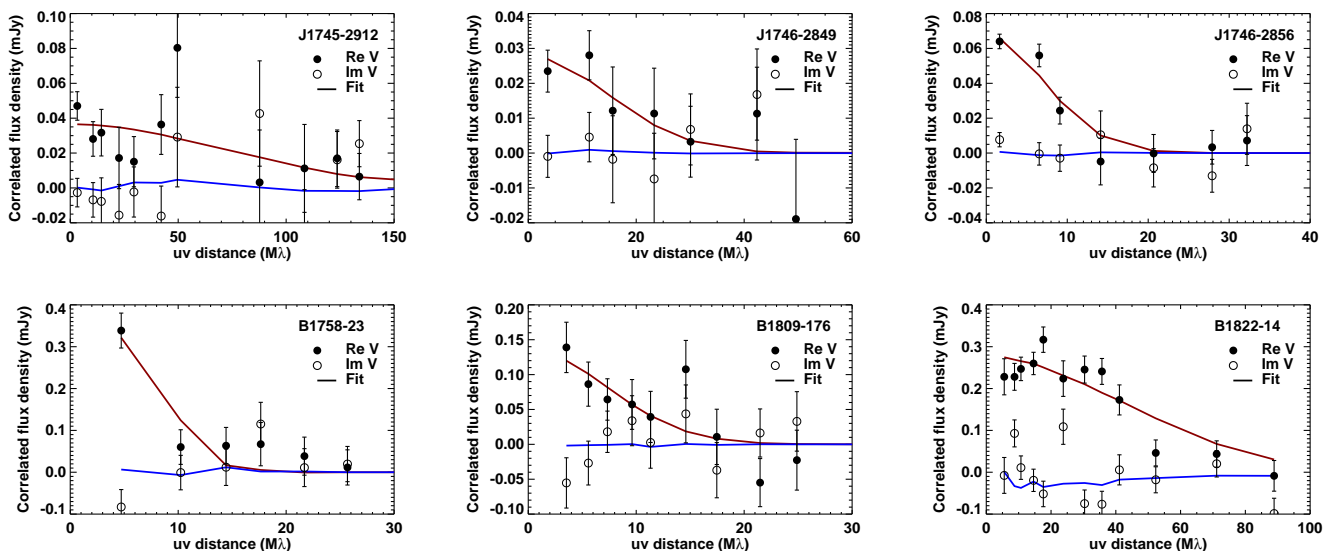
3 SIZE AND POSITION MEASUREMENTS

For the detected sources and using only the 8.7 GHz data for J1745–2912 (see above), we moved the phase centers of the visibilities to the source positions found in the cleaned images, and measured angular sizes and positions by fitting symmetric, offset Gaussian models to the complex visibility data, averaged over scans (typically $\simeq 20$ s). The parameter space over source flux density, angular FWHM size, and (x,y) position offset was sampled using a Markov Chain Monte Carlo (MCMC) algorithm as implemented in the publicly available EMCEE code (Foreman-Mackey et al. 2013). The likelihood was calculated assuming uniform priors on each parameter. A log(size) prior leads to marginally smaller size estimates ($< 1\sigma$) for the weakly detected sources. We also tried asymmetric (2D) Gaussian models, since the images seem to show asymmetric structure. However, asymmetry was not significantly detected for any object ($< 2\sigma$). This is probably a result of low signal-to-noise on individual baselines.

The best fitting models are compared to scan-averaged

Table 2. Flux densities (F_ν , from VLBI model fitting and VLA pulse profiles), FWHM sizes, and ICRF positions for detected sources.

Source	ν_{obs} (GHz)	RA	DEC	F_ν (mJy)	1σ range	Size (mas)	1σ range	VLA F_ν (mJy)
J1745-2912	8.7	17:45:47.83043(23)	-29:12:30.780(3)	0.037	[0.33, 0.42]	1.7	[0.3, 3.1]	0.056
J1746-2849	8.7	17:46:03.35736(12)	-28:50:13.385(2)	0.025	[0.021, 0.029]	5.3	[2.6, 8.0]	0.011
J1746-2856	5.9	17:46:49.85480(6)	-28:56:58.990(1)	0.067	[0.065, 0.071]	10.9	[9.7, 12.1]	0.11
B1758-23	7.5	18:01:19.81488(60)	-23:04:44.637(10)	0.41	[0.34, 0.45]	12.5	[10.3, 14.5]	
B1809-176	4.5	18:12:15.85925(17)	-17:33:37.871(2)	0.15	[0.09, 0.20]	17.6	[10.3, 24.7]	
B1822-14	7.5	18:25:02.95832(1)	-14:46:53.3605(2)	0.27	[0.26, 0.28]	1.8	[1.7, 2.0]	


Figure 3. Best fitting 1D offset Gaussian models (lines) compared to real (solid) and imaginary (open) visibilities for each source detected. For J1745–2912, we have shown the 8.7 GHz data, as described in the text. The amplitude shown is the equivalent period-averaged flux density for the pulsar, i.e. correcting for the gate width.

and uv-binned data in Figure 3. The uv-binning is done for presentation and was not included for fitting. The probability distributions over model parameters are shown in Figure 4 and the best fitting flux densities, source positions, and FWHM angular sizes along with 1σ confidence intervals are listed in Table 2.

As expected, the model fits identify sources close to the positions where they appear in our images in all cases. Source extension is detected in all cases, although with relatively low significance ($\simeq 90\%$) for J1746–2849 and J1745–2912. For J1746–2849, this is due to the faintness of the source. The size of J1745–2912 at 8.7 GHz is much smaller than the beam (e.g. Figure 2) and so the source is only partially resolved. Typical 1σ uncertainties are $\simeq 10 - 50\%$. Residual phase errors likely lead to systematic errors of comparable magnitude (§ 4.8).

The flux densities from model fitting are also generally compatible with (within a factor of 2 of) the expected values based on the known pulsar brightness and spectral index values (Table 1). In particular, PSR B1758–23 must have a relatively flat spectrum to be detected at 7.5 GHz. We also confirm the steep spectrum of PSR J1746–2856. For the GC sources, we can also compare to the independent VLA flux density estimates (§2.4). PSR J1746–2849 is found to

be significantly brighter in model fitting (factor of $\simeq 2.5$), while otherwise the agreement is good within errors.

The image centroids (source positions) in most cases are constrained to $\lesssim (2,4)$ mas. The best position constraint is for B1822–14 (0.1,0.2) mas, where the detection significance is very high and the source is compact. The precision is lower for more extended sources (1,2) mas for J1746–2856, J1746–2849, and B1809–176), and lower still for J1745–2912 where the size is poorly constrained (2,4) mas. For B1758–23, phase errors lead to an elongated streak in the image and multiple solutions for the source position reaching out to tens of mas offsets from the cleaned image peak. Despite this issue the 1D source size remains well constrained. The *accuracy* of the source positions is limited to $\gtrsim 1$ mas by the precision of the phase calibrator position in the ICRF. The measured flux densities and angular sizes are consistent with the images and with fits to uv-binned or time-averaged data.

All three GC pulsar locations are in good agreement with those from recent ATCA observations (Schnitzeler et al. 2016), with offsets $\lesssim (0.020, 0.2)$ arcsec. The offsets from previous pulsar timing positions, both for GC and non-GC sources, are larger: $\lesssim (0.3, 0.6)$ arcsec, but generally in agreement within errors. For B1809–176 the

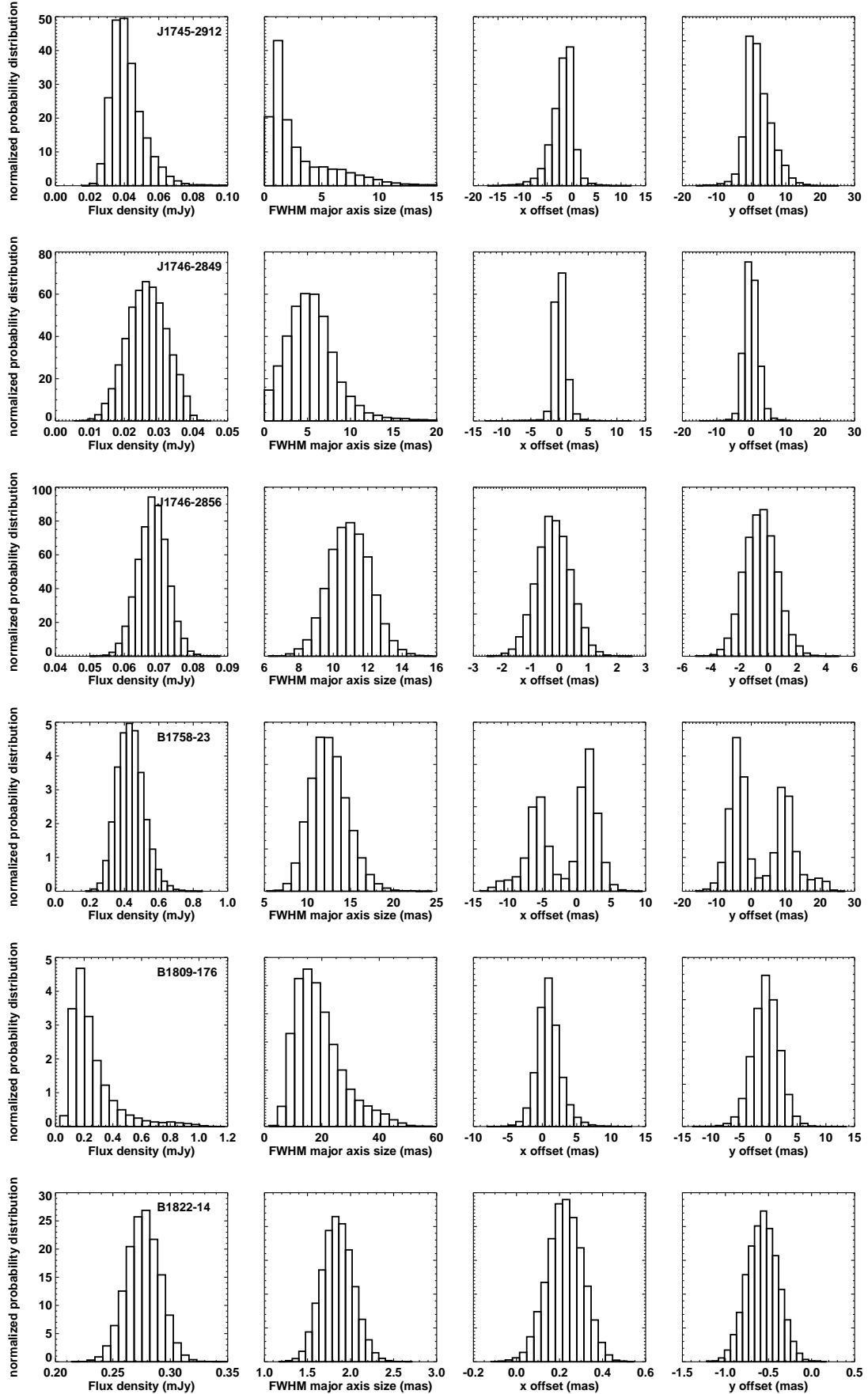


Figure 4. Probability density as a function of total flux density, FWHM Gaussian size, and x and y offset from image centroid for all detected sources from fitting a symmetric Gaussian model to the scan-averaged calibrated visibilities. An extended source is detected in each case at a small offset from the image source position.

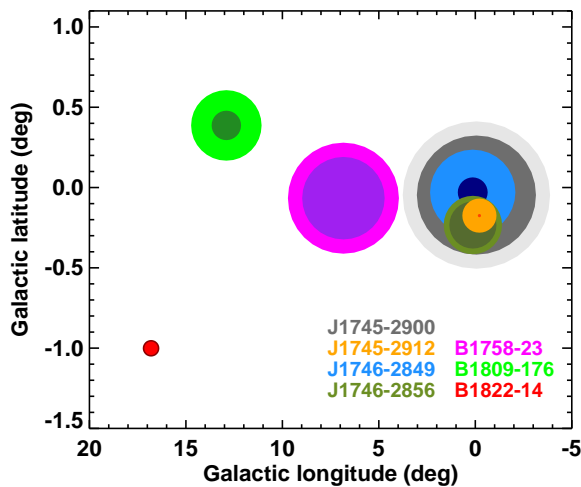


Figure 5. Measured $\pm 1\sigma$ angular size ranges (radii of the inner and outer circles) vs. Galactic coordinates (l, b), scaled to the angular broadening of the GC magnetar SGR J1745–2900 (gray, Bower et al. 2014). The other GC sources are significantly smaller in angular extent than J1745–2900 and Sgr A*, while B1758–23 is comparable in angular size.

RA offset is $\simeq 4\sigma$ from the pulsar timing position and for B1822–14 both offsets are $\simeq 2\sigma$.

Our VLBA+VLA measurements used Sgr A* as a secondary phase calibrator, and so included the GC magnetar SGR J1745–2900 as well. Its angular size is found to agree with previous measurements (Bower et al. 2014, 2015). Claussen et al. (2002) previously constrained the size of B1758–23 to be < 0.5 arcsec at 1 GHz. Scaling our results to this frequency assuming $\theta \propto \nu^{-2}$ gives $\theta \simeq 0.7 \pm 0.2$ arcsec, marginally compatible with their result. A flatter scaling (see § 4.1) leads to better agreement.

4 MAPPING STRONG INTERSTELLAR SCATTERING

Figure 5 shows the angular sizes of the sources measured here as a function of Galactic coordinates, scaled to the size of SGR J1745–2900 at the observing frequency (equivalent to assuming $\theta \propto \nu^{-2}$). Sgr A* and SGR J1745–2900 have been found to have the same scatter-broadened image in size, position angle, and frequency-dependence (Bower et al. 2014). We show the scattering properties of SGR J1745–2900 as a reference in what follows, assuming that they are identical to those of Sgr A*.

The sources in the GC are all found to be smaller in angular size than SGR J1745–2900. J1746–2849 and J1746–2856 are a factor $\simeq 2-3$ smaller, while the very compact 8.7 GHz size of J1745–2912 is several times smaller. These variations in angular size are comparable to those among the known OH/IR masers (van Langevelde et al. 1992; Frail et al. 1994; Yusef-Zadeh et al. 1999) and extragalactic background sources (Lazio et al. 1999; Bower et al. 2001) at similar separations. Outside of the GC, the pulsar B1758–23 has a large angular size, comparable to that of Sgr A*, despite a smaller τ and DM by factors $\simeq 2$.

The other sources are significantly less scattered. B1809–176 still shows significant angular broadening, while B1822–14 is compact.

In the following, we combine these new angular broadening measurements with distance and temporal broadening values from the literature to locate the scattering along the line of sight. We then identify candidate origins for the scattering by comparing these locations with those of known HII regions and supernova remnants.

4.1 Temporal broadening and distance data

We use existing data for the temporal broadening and distances to the pulsars in our sample (Table 3). The literature data come first from the ATNF catalog (Manchester et al. 2005) and references within, and further include more recent, multi-frequency measurements (Lewandowski et al. 2013, 2015). The GC pulsars are assumed to be located at the distance of the GC, which we fix at 8.3 kpc (Reid et al. 2014; Chatzopoulos et al. 2015; Gillessen et al. 2017). The pulsar B1758–23 has a recent distance measurement of 4 ± 1 kpc from HI absorption (Verbiest et al. 2012). For PSRs B1809–176 and B1822–14 we use DM distances from the NE2001 model (Cordes & Lazio 2002). Distances predicted using Galactic electron density distribution models depend on the model employed; using the recent YMW17 model (Yao et al. 2017) in place of NE2001 predicts significantly smaller distances for these two pulsars, which we find to be more consistent with our scattering data. However, in estimating screen locations from our data we find insignificant (< 0.3 kpc) differences from the choice of DM distance.

From the literature data, we estimate τ at the observing frequencies used for our size estimates. This involves extrapolation: τ is difficult to measure at high frequencies like those used for the VLBA+VLA observations, which are required in order to match the array resolution to the large image sizes.

We extrapolate τ to the VLBA+VLA observed frequency using a spectral index $\tau \propto \nu^{-\alpha}$. For a single, infinitely extended, thin scattering screen this value is $\alpha \geq 4$, where $\alpha = 4.4$ for Kolmogorov turbulence and $\alpha = 4$ for a finite turbulent inner scale (Goodman & Narayan 1985). When these model assumptions break down, the frequency scaling is flatter (Cordes & Lazio 2001), as seen for many high DM pulsars (average $\alpha \simeq 3.5$, Löhmer et al. 2001) like those imaged here. When multiple measurements of τ are available, we use the measured spectral index and account for the extrapolation error in our final estimate of τ at our observing frequency. When only a single value is available (PSR J1745–2912¹ and PSR B1809–176), we assume $\alpha = 4 \pm 0.5$ to extrapolate. The values of α assumed, their errors, and resulting τ estimates and errors are shown in Table 3. For J1746–2849, the published values (Deneva et al. 2009) show a very flat slope $\alpha \approx 2.2$. An upper limit on $\tau \lesssim 5$ ms at 5 GHz comes from the observed pulse width. Adding this limit leads to an estimate of $\alpha = 3.3 \pm 0.3$. For

¹ We tried to measure τ at 5.6 GHz from the tied-array VLA data. A value of $\simeq 2-3$ ms is compatible with the data, but the result depends on the assumed intrinsic profile. A value > 3 ms seems unlikely, implying a slope $\alpha \gtrsim 3.5$.

Table 3. Multi-frequency temporal broadening, $\tau(\nu_\tau)$, and distance (D) data used, and our extrapolation of the temporal broadening data to the observed frequency of the VLBI observations, $\tau(\nu_{\text{obs}})$, using a spectral index $\tau \propto \nu^{-\alpha}$.

ν_τ (GHz)	τ (ms)	α	ν_{obs} (GHz)	$\tau(\nu_{\text{obs}})$ (ms)	D (kpc)	D_{NE2001}	D_{YMW17}	Refs.
J1745–2912								
3.1	25 ± 3	4 ± 0.5	8.7	$0.4^{+0.3}_{-0.2}$	8.3	15	8.1	6,8,9,10,12
J1746–2849								
1.5	266	3.3 ± 0.3	8.7	$0.9^{+0.7}_{-0.3}$	8.3	30	8.2	6,9,10,11,12
2.0	140							
J1746–2856								
1.4	170 ± 15	3.07 ± 0.14	5.9	2.0 ± 0.4	8.3	8.4	8.2	6,8,9,10,12
3.1	15 ± 2							
B1758–23								
1.275	130.5 ± 5.4	3.5 ± 0.2	7.5	0.27 ± 0.10	4 ± 1	12	6.5	1-5,12
1.374	102.5 ± 1.1							
1.400	99 ± 19							
1.400	111 ± 19							
1.421	83.2 ± 3.9							
1.518	74.3 ± 1.3							
1.642	51 ± 10							
1.642	55 ± 10							
2.263	17.9 ± 0.8							
2.600	0.75 ± 0.34							
2.700	8.6 ± 1.7							
4.850	0.23 ± 0.08							
B1809–176								
1	$5.89 \pm 20\%$	4 ± 0.5	4.5	$0.14^{+0.14}_{-0.07}$	6.3 ± 0.6	6.3	4.5	6,7,12
B1822–14								
0.610	143 ± 31	3.8 ± 0.4	7.5	$0.010^{+0.007}_{-0.005}$	5.5 ± 0.5	5.5	4.5	3,6,12
1.060	15.1 ± 2.0							
1.400	6.1 ± 1.2							
1.642	3.7 ± 1.5							

Reference key: (1) Manchester et al. (1985) (2) Löhmer et al. (2001) (3) Lewandowski et al. (2013) (4) Lewandowski et al. (2015) (5) Verbiest et al. (2012) (6) Cordes & Lazio (2002) (7) Manchester et al. (2005) (8) Johnston et al. (2006) (9) Chatzopoulos et al. (2015) (10) Gillessen et al. (2017) (11) Deneva et al. (2009) (12) Yao et al. (2017)

Table 4. Screen distance D_s calculation results from our observations compared to those of J1745–2900.

Name	ν (GHz)	τ (ms)	D (kpc)	θ (mas)	D_s (kpc)
J1745–2912	8.7	$0.4^{+0.3}_{-0.2}$	8.3	1.7 ± 1.4	8.0 ± 0.3
J1746–2849	8.7	$0.9^{+0.7}_{-0.3}$	8.3	5.3 ± 2.7	7.4 ± 0.7
J1746–2856	5.9	2.0 ± 0.4	8.3	10.9 ± 1.2	6.9 ± 0.3
B1758–23	7.5	0.27 ± 0.10	4 ± 1	12.4 ± 2.1	2.0 ± 0.5
B1809–176	4.5	$0.14^{+0.14}_{-0.07}$	6.3 ± 0.6	17.5 ± 7.2	1.0 ± 0.7
B1822–14	7.5	$0.010^{+0.007}_{-0.005}$	5.5 ± 0.5	1.85 ± 0.15	2.9 ± 0.8
J1745–2900	8.7	0.35 ± 0.10 (1)	8.3	12.5 ± 1.2 (2)	3.1 ± 0.6

(1) Spitler et al. (2014) (2) Bower et al. (2014)

B1758–23, Lewandowski et al. (2013) reported a steep dependence $\alpha = 4.92$ using a mix of low- and high-frequency data. Lewandowski et al. (2015) removed the high-frequency data and found a shallower slope $\alpha = 3.62$. We use the latter measurement, which is consistent with the result of Löhmer et al. (2001), and note that τ could be smaller if the high-frequency data are more accurate. We further assume 10% DM distance uncertainties (Cordes & Lazio 2002), but they do not strongly affect the results. Section 4.8 includes additional discussion of the systematic errors from extrapolating τ and using DM distances.

4.2 Locating scattering screens

Given angular and temporal broadening measurements at the same frequency to the same source, the single thin screen scattering model gives a location for the scattering medium of (Cordes & Lazio 1997),

$$\frac{\Delta}{D} = \left(1 + \frac{8c\tau \ln 2}{D\theta^2}\right)^{-1}, \quad (1)$$

where Δ is the distance from the source to the scattering medium, D is the source distance, τ is the pulse broadening decay constant $\propto e^{-t/\tau}$, and θ is the angular broadening

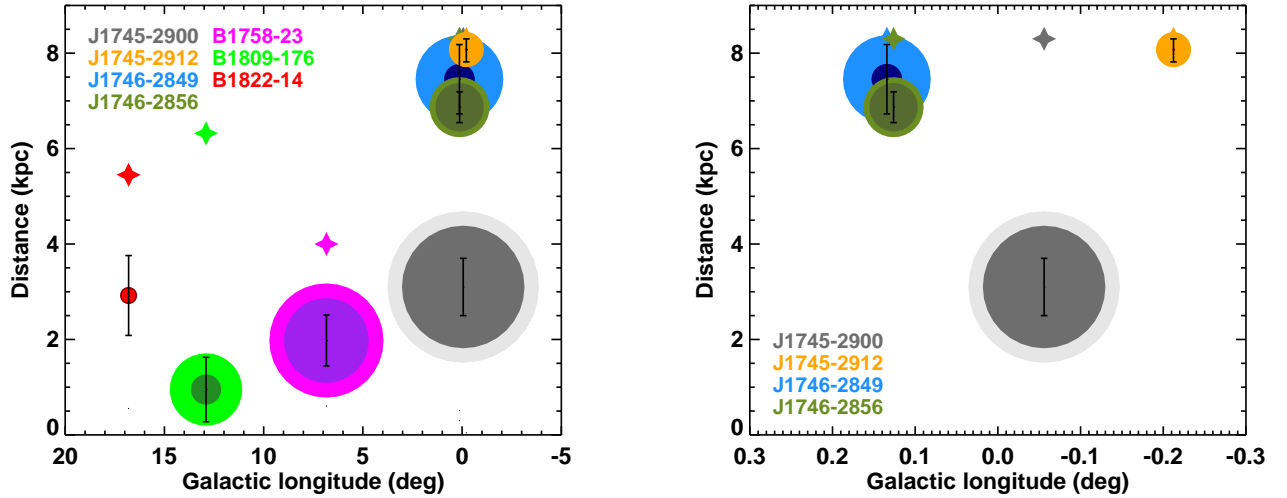


Figure 6. Measured $\pm 1\sigma$ angular size ranges (radii of the inner and outer circles, scaled to the size of the GC magnetar in gray) vs. Galactic longitude and distance from Earth for all detected sources (left) and zooming in on the GC sources (right). The stars show the location of the pulsars, while the circles are placed at the scattering location $D_s = D - \Delta$ found from the combined angular and temporal broadening (equation 1). The sources near the GC are assumed to be located at the distance of Sgr A* (Chatzopoulos et al. 2015), while the DM distance is used for the remaining sources. The location of the scattering towards all 3 non-GC sources detected is consistent with a nearby spiral arm. The scattering towards the other GC sources is inferred to occur much closer to the GC than in the case of Sgr A* and SGR J1745–2900. The very small size of J1745–2912 implies $\Delta \lesssim 700$ pc, direct evidence for a strong scattering medium in the GC.

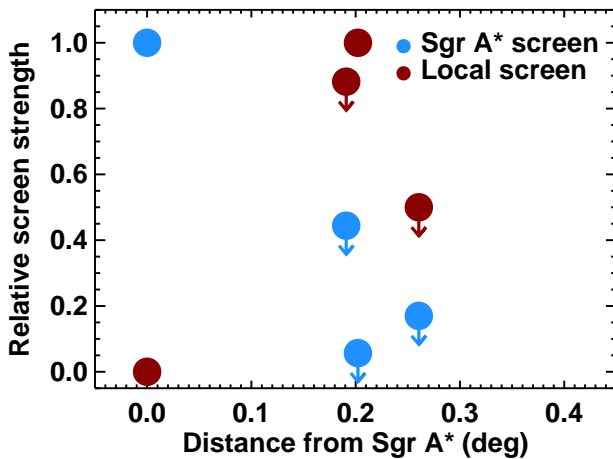


Figure 7. Maximum fraction of the temporal broadening of the GC pulsars (blue points) that could be produced at the scattering location of J1745–2900, $\Delta \simeq 5$ kpc from the GC (Spitler et al. 2014; Bower et al. 2014), as a function of their angular separation. The scattering source for the magnetar and Sgr A* weakens or disappears on scales $\lesssim 0.2$ deg. The bulk of the temporal broadening for these pulsars must have a different physical origin, closer to or residing within the GC. The maximum relative strength of a possible screen local to the GC, suggested by the small tentative size measurement of J1745–2912, is shown as the red points. The two screen model (red and blue points) constitutes the minimal assumption needed to explain all GC pulsar observations. The upper limits take into account models with additional components.

in terms of FWHM Gaussian image size. Using existing τ measurements and distance estimates (above and Table 3), we infer scattering locations $D_s = D - \Delta$ for all objects in our sample.

To find median values for D_s and its uncertainty for each pulsar, we draw random Gaussian samples for τ , θ (using our measured 1σ errors from §3), and D , calculate D_s for each sample, and measure 1σ confidence intervals based on their distributions. The resulting D_s values are listed in Table 4. The values from previous work for the GC magnetar are also there, where we have extrapolated τ as above. Using our method we find $D_s = 3.1 \pm 0.6$ kpc, compared to $D_s = 2.6 \pm 0.3$ kpc from Bower et al. (2014). The values are consistent within 1σ . Ours is slightly larger and with larger uncertainty due to extrapolating τ with $\alpha = 3.8 \pm 0.2$ Spitler et al. (2014) rather than $\alpha = 4$ in Bower et al. (2014).

Figure 6 again shows the measured source sizes, but now as a function of Galactic longitude and line of sight distance. The vertical error bar shows the scattering location D_s and its uncertainty. The measurement for SGR J1745–2900 (Bower et al. 2014) is closer to Earth than the inferred scattering locations for the other GC pulsars. This is due to their relatively small angular sizes and large τ values compared to those of the magnetar. The very compact 8.7 GHz size and large τ for J1745–2912 would place its scattering local to the Galactic center: $\Delta < 700$ pc. This is tentative evidence for strong scattering from the hot, dense medium within the GC itself. The other GC pulsars have scattering media $\simeq 7$ kpc from Earth. That location could either arise from a single scattering origin at that location, or from a combination of distant scattering similar to the magnetar and local scattering as seen for J1745–2912.

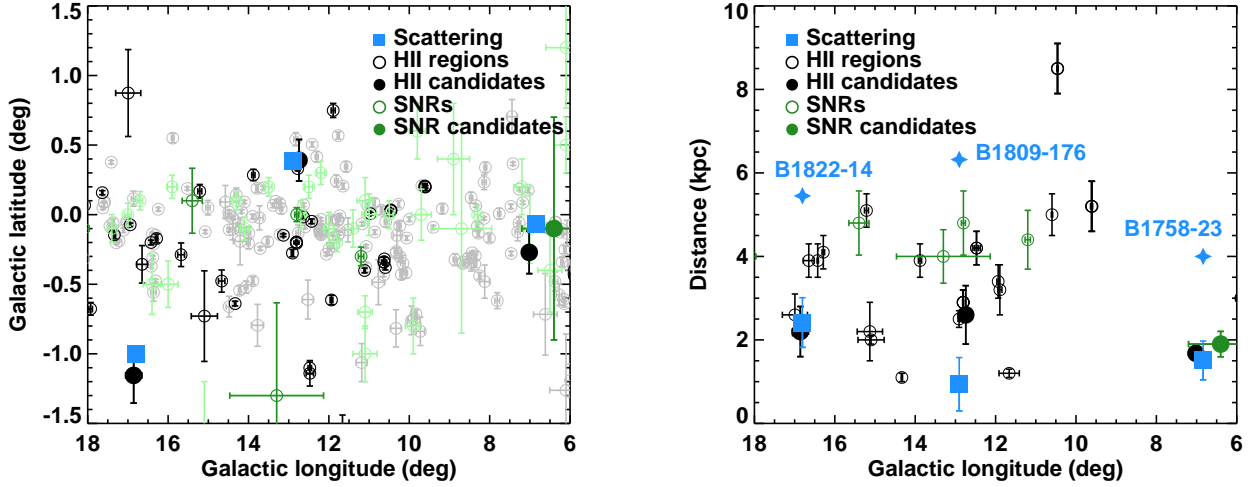


Figure 8. Scattering locations towards the non-GC pulsars in our sample (light blue squares) and the pulsars themselves (light blue stars, right panel) compared with the positions of known HII regions (open black points, [Anderson et al. 2014](#)) and supernova remnants (open green points, [Green 2014](#)) in Galactic longitude and latitude (left) and Galactic longitude vs. distance (right). The error bars in Galactic coordinates correspond to the measured sizes of the objects, while the error bar in the distance is its uncertainty. In the right panel we only show objects for which distances are given in the catalogs (darker points in the left panel). We identify candidates (solid circles) as sources overlapping with the (l,b) position of our pulsars. In all cases, these sources have distances commensurate with our inferred distance to the scattering medium in front of the pulsars. For all three objects, an HII region has the right distance to produce the observed scattering. For B1758–23, the supernova remnant W28 is also at the inferred scattering location (but closer to Earth than PSR B1758–23, see figure 9).

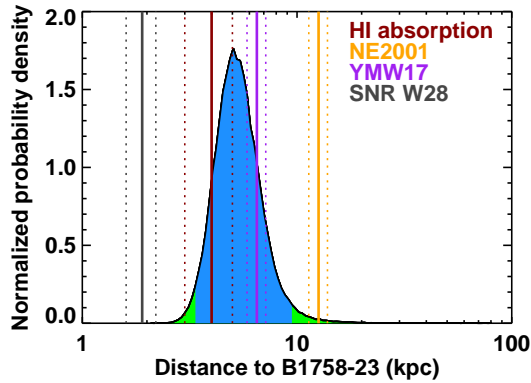


Figure 9. Probability distribution for the distance to the pulsar B1758–23 measured from combining its temporal and angular broadening (Table 3) with the angular broadening of the nearby extragalactic background source J1801-231 ([Claussen et al. 2002](#)), assuming the two sources are behind a common, thin scattering medium. The resulting distance estimate (blue shaded region shows 2σ confidence interval) is consistent with the recent measurement of 4 ± 1 kpc from HI observations ([Verbiest et al. 2012](#)) and the recent DM distance from [Yao et al. \(2017\)](#), but smaller than the prediction of the NE2001 model ([Cordes & Lazio 2002](#)). This distance is also incompatible with an association of the pulsar with the supernova remnant W28 at a distance 1.9 ± 0.3 kpc ([Velázquez et al. 2002](#)), although this SNR could contribute to its scatter broadening (Figure 8).

The non-GC pulsars all have $D_s \simeq 1 - 2$ kpc, consistent with locations in the Carina-Sagittarius or Scutum spiral arm and similar to or closer than the scattering medium

producing the image of the GC magnetar. The large size of B1809–176 implies a scattering location $\simeq 1$ kpc from Earth. As discussed below, the nearest candidate sources are closer to $\simeq 2.5$ kpc. The size could be overestimated, the τ value could be underestimated (see also §4.8), or the scattering could have some other physical origin.

4.3 Multiple scattering origins towards the GC

The sizes of scatter-broadened maser and extragalactic background sources within $\simeq 0.5$ deg of Sgr A* have long been known to vary by factors of several (e.g., [van Langevelde et al. 1992](#); [Frail et al. 1994](#); [Yusef-Zadeh et al. 1999](#); [Lazio et al. 1999](#); [Bower et al. 2001](#); [Pynzar’ 2015](#)). Our finding of small angular sizes for GC pulsars with large degrees of temporal broadening demonstrates that these variations are not only the result of varying strength in a single scattering medium. Instead, they require (at least) a second physical component to the scattering. The small size found for J1745–2912, if it holds, suggests this component could be located within the GC itself ($\Delta < 700$ pc). The existence of such a component has long been suggested (e.g., [Cordes & Lazio 1997](#)), but with τ a factor $\sim 10^{2-3}$ higher than that of the known GC pulsars. Our sample selection of known pulsars detected at GHz frequencies means that none of the identified scattering screens can be responsible for obscuring long period pulsars in the GC.

Phase-resolved angular broadening of the pulses of J1745–2900 shows that the scattering appears to be dominated by a single thin scattering screen ([Wucknitz 2015](#)). In calculating screen locations (D_s), we have assumed this to be true separately for each of the other pulsars as well. Instead

we now consider the minimal model needed to explain all of the GC pulsar scattering measurements. The model consists of two scattering origins, one local to the GC ($\Delta < 700$ pc to explain the small size of J1745–2912) and one at $\Delta \simeq 5$ kpc as inferred for the magnetar. For simplicity we assume that the local GC screen only contributes to τ and not θ , while the other contributes to both as described by equation (1). In this scenario, we calculate the contribution to the τ of our GC pulsars from the distant screen and from the local GC screen in order to produce their observed angular broadening. These contributions are shown in Figure 7 (red and blue filled circles), scaled to the 1.3s τ measurement for J1745–2900 (Spitler et al. 2014) and to the $\tau \simeq 2.3$ s at 1 GHz of J1745–2912 (Deneva et al. 2009). By definition the magnetar and J1745–2912 only have contributions from the distant and GC screens respectively. This minimal model sets robust upper limits on the contributions of the two components to the angular broadening of each pulsar. The limits (shown in the figure) generalize to include models with additional scattering components.

The simple model robustly shows that the distant GC screen drops significantly in relative strength at the location of the other GC pulsars, particularly for J1745–2912 because of its very small size, but also (robustly) for J1746–2856 where the size is well constrained. The constraint for J1746–2849 is weaker, because the size is more weakly constrained. Conversely, the local GC screen does not appear to contribute significantly at the location of J1745–2900, since the scattering is well explained by a single screen, but could produce a large fraction of the observed temporal broadening for the other GC pulsars given their scattering locations in or near the GC. The observed maser sources (e.g., van Langevelde et al. 1992; Frail et al. 1994) are heavily scatter-broadened out to scales of $\simeq 0.5$ deg, larger than the scale over which the two components vary greatly in strength. The physical medium responsible for scattering Sgr A* and the magnetar cannot be responsible for all of intense scattering towards the GC on this scale.

The pulsar J1746–2856 at a separation $\simeq 0.2$ deg has a scattering location $\simeq 1 - 2$ kpc from the GC. In the two-component model this would be caused by contributions from the local GC and distant screens. Instead, it could be due to a separate, single thin screen at $D_s \simeq 7$ kpc (figure 6), compatible with a location in the inner spiral arms as well as near the GC region (e.g., possibly the 3 kpc arm, Sanna et al. 2014). Our observations cannot distinguish between these possibilities. The weak constraint for PSR J1746–2849 leaves it compatible with the scattering location of either J1745–2912 or J1746–2856.

4.4 Associations with known HII regions

We checked the lines of sight towards our pulsars against catalogs of HII regions (Anderson et al. 2014; Lockman 1989) and supernova remnants (SNRs, Green 2014) in the inner Galactic plane. The sources are shown compared to the 3D scattering locations for each non-GC pulsar in Figure 8. From the WISE catalog, we identify one promising candidate HII region for each of B1809–176 and B1822–14 with separation comparable to the measured radius (S30 and S40, Sharpless 1959). Additionally, the line of sight to-

wards B1758–23 is close to ($\lesssim 5$ pc from) the Trifid Nebula at a distance $\simeq 1.8$ kpc, which hosts an O star with a large HII region (S50, Lynds & Oneil 1985; Cordes & Lazio 2003). This region may also be interacting with the SNR W28 at a distance $\simeq 2$ kpc (e.g., Velázquez et al. 2002).

In all three cases, the candidate sources overlapping in the sky plane are located at distances commensurate with the scattering locations D_s inferred for the pulsars. The association of the scattering medium with these HII regions (and/or the SNR in the case of B1758–23) therefore seems likely. For the GC sources, there are no known candidate HII regions on the line of sight towards J1745–2912, while J1746–2849, J1746–2856, and SGR J1745–2900 are covered by at least one candidate HII region. However, claiming associations between the HII regions and GC scattering is difficult. Kinematic distances cannot be determined towards the GC, and the region is crowded with sources both along the lines of sight and within the GC region.

Interstellar scattering has also been proposed to originate at the ionized outer regions of giant molecular clouds. The line of sight to two of the non-GC pulsars pass near the edge of the candidate HII regions, possibly consistent with this scenario.

4.5 The distance to B1758–23

The extragalactic background source J1801-231 is only 2 arcminutes from B1758–23 in angular separation. Claussen et al. (2002) showed that its angular size $\theta \sim \nu^{-2}$ or steeper, as predicted for scatter-broadening. Assuming that B1758–23 and J1801-231 share a single, thin scattering medium, those constraints along with the temporal broadening of the pulsar provide unique solutions for the distance to the scattering medium and to the pulsar:

$$D_s = 2.292 \frac{\tau_p}{\theta_p \theta_{\text{ex}}}, \quad (2)$$

$$D = \frac{D_s}{1 - \theta_p / \theta_{\text{ex}}}, \quad (3)$$

where D and D_s are in kpc, τ_p is in seconds, θ_{ex} and θ_p are in arcseconds, and all quantities are measured at a common frequency.

Using our measurement of the size of B1758–23, we repeat this exercise. The quantities θ_{ex} and τ_p have both been measured up to a frequency $\nu \simeq 1.7$ GHz. We then need to extrapolate our measured size back in frequency. In order to remain consistent with our assumptions for measuring D_s in §4.2, we scale $\theta_p^2 \propto \tau_p$, using $\tau_p \propto \nu^{-\alpha}$ with $\alpha = 3.5 \pm 0.2$ (Table 3). At 1.7 GHz, the values assumed are then $\tau_p = 47 \pm 7$ ms, $\theta_{\text{ex}} = 275 \pm 25$ mas, and $\theta_p = 160 \pm 60$ mas. We again draw random Gaussian samples to measure a new $D_s = 2.3 \pm 0.6$ kpc, consistent with the measurement above. The extragalactic source size measured by Claussen et al. (2002) is therefore consistent with a shared scattering origin with PSR B1758–23.

The difference between pulsar and extragalactic source sizes can then be used to estimate the distance to the pulsar. The resulting value is $D = 5.3^{+1.4}_{-1.1}$ kpc, consistent with the HI distance used in §4.2. The probability distribution over D is shown in Figure 9. Large distances $\simeq 10$ kpc, as found in NE2001 due to the large pulsar DM, are disfavored

at $> 2\sigma$. The measured distance rules out ($> 3\sigma$) an association of PSR B1758–23 with the supernova remnant W28 at a distance $D \simeq 2$ kpc (e.g., Goss 1968; Arikawa et al. 1999; Velázquez et al. 2002). The supernova remnant is at a distance compatible with D_s and so could contribute to the observed scattering (§4.4).

4.6 B1822–14 proper motion

Moldón et al. (2012) used VLBA observations of B1822–14 at 5 GHz from 2009–2011 to measure its proper motion to be $\mu_\alpha \cos \delta = 10.0 \pm 0.3$ mas yr^{−1}, $\mu_\delta = -29.0 \pm 0.3$ mas yr^{−1}. Figure 10 shows their data, archival VLA data (Frail & Scharringhausen 1997), and our new data point, along with fits for the proper motion and the residuals. All VLBA observations used the common phase reference source J1825–1718, and we correct all measurements to reflect the latest measured calibrator position. To account for systematics due to the different observing frequencies used (5 vs. 7.5 GHz), for example due to core shift of the calibrator source, an extra 0.5 mas error has been added to our data point. The updated fit is

$$\begin{aligned} \alpha_{J2000} &= 18^{\text{h}}25^{\text{m}}28^{\text{s}}.955067 \pm 0.29 \pm 0.12 \text{ mas}, \\ \delta_{J2000} &= -14^{\circ}46'53''.24531 \pm 0.26 \pm 0.17 \text{ mas}, \\ \mu_\alpha \cos \delta &= 11.07 \pm 0.10 \text{ mas yr}^{-1}, \\ \mu_\delta &= -27.61 \pm 0.10 \text{ mas yr}^{-1}, \end{aligned}$$

where the weighted reference epoch is Oct. 20, 2011 (MJD 55854.7) and the second error terms are the current calibrator position uncertainties in the ICRF. The fit result is poor: reduced $\chi^2 = 4.1$. As can be seen from the residuals in figure 10, there is a systematic $\simeq 2$ mas offset between their final measurement and ours. This explains the discrepancy between the proper motion measurements at the $\simeq 3 - 4\sigma$ level. The residuals are likely due to underestimated systematics in comparing the positions, which could result for example from a larger than average core shift or refractive image wander from scattering. On the other hand, we can rule out their measured proper motion, since it would lead to an offset of $\simeq 8$ mas in both RA and Dec from the current position of PSR B1822–14. Future VLBI observations at 7.5 GHz, as used here, would allow a more robust proper motion measurement. In any case, we have verified the large proper motion of this pulsar seen by Moldón et al. (2012). At the estimated DM distance of $\simeq 5.5$ kpc, this corresponds to a space velocity of $\simeq 750$ km s^{−1}, confirmation that B1822–14 is a runaway pulsar.

4.7 Large DM contributions from single HII regions and effect on distance estimates

Assuming that the nearby HII regions above are responsible for the observed temporal and angular broadening, we estimate the minimum electron number density required to produce the observed images at the inferred screen locations.

For scattering by a thin screen of material with a Kol-

mogorov turbulent spectrum and inner/outer scales $L_{0,1}$, the image size is given by (van Langevelde et al. 1992):

$$\theta = \frac{\pi \rho_C}{\sqrt{2 \ln 2} \lambda}, \quad (4)$$

where θ is the FWHM size as measured here,

$$\rho_C = \left[6\pi^2 \lambda^2 r_e^2 \mathcal{L}(D) q_1^{1/3} \right]^{-1/2}, \quad (5)$$

and

$$\mathcal{L}(D) = \int_0^D dx C_n^2(x) \left(\frac{x}{D} \right)^2, \quad (6)$$

where C_n^2 is the normalization of the turbulent power spectrum.

A lower limit to the average electron number density required to produce an observed image size comes from assuming the density fluctuations are order unity, $\delta n_e = n_e$, so that,

$$n_e \geq \delta n_e = (6\pi C_n^2)^{1/2} \left(\frac{L_0}{2\pi} \right)^{1/3}. \quad (7)$$

For the individual HII regions associated with these scattering screens, we follow Sicheneder & Dexter (2017) and set the line of sight distance through the cloud to its measured radius, R , and the outer scale to $L_0 = f_2 R$, where $f_2 \leq 1$ is an unknown constant.

The density can then be written as,

$$n_e \simeq 130 \left(\frac{\theta}{10 \text{ mas}} \right) \left(\frac{\nu}{7.5 \text{ GHz}} \right)^{-2} \left(\frac{R}{3 \text{ pc}} \right)^{1/6} \gamma^{-1} f_2^{-1/3} \text{ cm}^{-3}, \quad (8)$$

where $\gamma = \Delta/D$ is the screen location and we have assumed an inner scale of $L_1 = 10^4$ km (e.g., Wilkinson et al. 1994).

For the three non-GC pulsars with associated HII regions S30/S40/S50, we can estimate the minimum contribution from the HII regions to the DM, $\Delta\text{DM} = \eta n_e R$, where $\eta = 0 - 2$ is the fraction of R intersected by the line of sight. For parameter ranges of $f_2 = 1/10 - 1/2$, $\eta = 1/2 - 1$, we find $\Delta\text{DM} \simeq 250 - 1000$, $120 - 500$, $60 - 250$ pc cm^{−3} for B1758–23, B1809–176, and B1822–14 respectively. These lower limits are $\simeq 25 - 100\%$ of the total DM in each case.

The Trifid nebula, lying close to the line of sight to B1758–23 and at the distance we infer for the scattering, is ionized by the O7V star HD 164492A. For our $n_e \simeq 130 - 220$ cm^{−3} values for B1758–23 and the measured $R \simeq 4.5$ pc, we can use the Strömgren radius to calculate the photon flux, N_{Ly} , required to ionize the HII region:

$$N_{\text{Ly}} = 4/3\pi R^3 n_e^2 \alpha_H \simeq 0.7 - 2.0 \times 10^{50} \text{ s}^{-1}, \quad (9)$$

consistent with expectations for this stellar type (Sternberg et al. 2003), and estimates based on the observed continuum radio emission. The n_e values we find also agree with the measurement $n_e = 250 \pm 100$ cm^{−3} from line ratios (Lynds & Oneil 1985).

Dispersion measures are frequently used to infer pulsar distances (Taylor & Cordes 1993; Cordes & Lazio 2002).

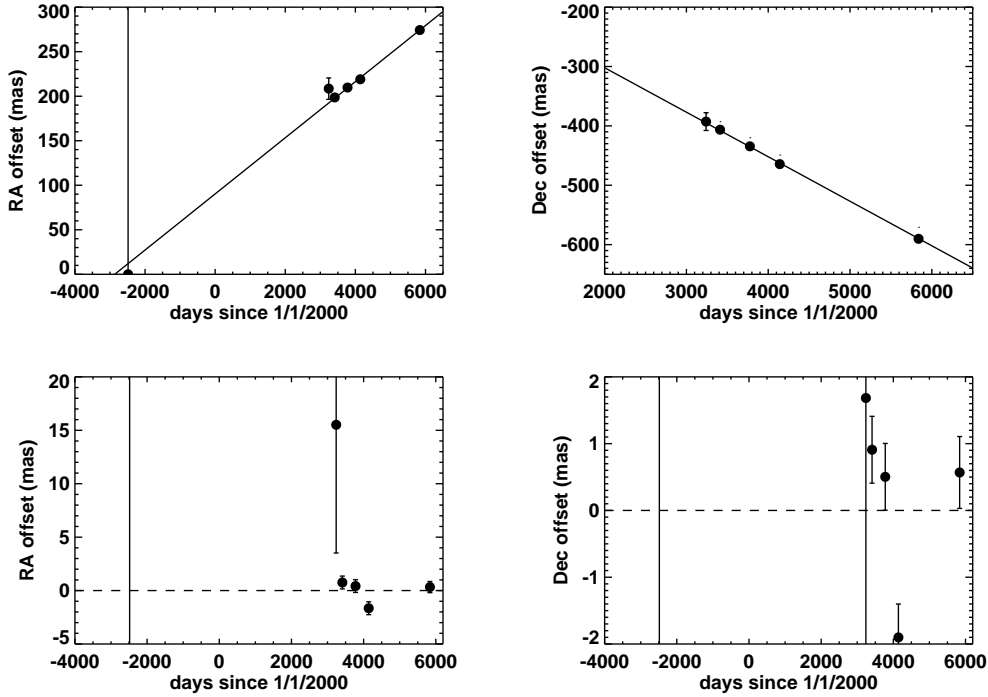


Figure 10. Proper motion of PSR B1822–14 in RA and Dec (top two panels) and the residuals of the VLBI data compared to the best linear fit (bottom two panels). The first two epochs are from archival VLA data (Frail & Scharringhausen 1997), the next four are VLA and VLBA observations (Moldón et al. 2012), and the final point is from our recent VLBA observation. Our position is consistent with the proper motion measured by Moldón et al. (2012).

The NE2001 model includes contributions from “clumps” of electrons along many lines of sight, including B1758–23. However, the contribution to the DM is assumed to be $\simeq 18 \text{ pc cm}^{-3}$ (Cordes & Lazio 2003), a factor $\gtrsim 10$ smaller than we infer would be the minimum contribution of the Trifid Nebula. These large DM contributions could therefore significantly reduce the inferred distances to pulsars located behind HII regions, an effect seen previously in the Gum nebula (Johnston et al. 1996). Using the NE2001 model, we calculate revised distances by subtracting a fiducial HII region contribution of 50% of the total DM. The new distances are 6.1, 3.8, and 3.8 kpc compared to NE2001 values of 12.6, 6.2, and 5.1 kpc. The revised distance estimate for B1758–23 of 6.1 kpc is comparable to that of 4 ± 1 kpc from HI absorption, and agrees with our estimate in §4.5. The revised estimates are also in good agreement with the new electron density model of Yao et al. (2017). Including these large DM contributions from known HII regions with density and radius could improve distance estimates for some lines of sight through the Galactic plane.

4.8 Systematic uncertainties

The measured sizes, extrapolated τ values, and source distances are all subject to systematic errors, which could exceed the statistical errors adopted in our analysis. Here we briefly discuss how those errors could affect the results.

4.8.1 Phase calibration errors and source sizes

The VLBA observations used phase referencing to nearby calibrator sources. However, the intense scattering to the Galactic plane often led to large offsets $\simeq 2 - 3^\circ$ to the nearest suitable calibrator source, which was sometimes still significantly scatter-broadened. Both effects can lead to residual phase errors which would cause us to overestimate the angular broadening of the target sources. During the observations of PSR J1745–2912, we also observed Sgr A* using the same phase reference calibrator. The images of Sgr A* formed without self-calibration were broadened by $\sim 50\%$ compared to the expected size, which was recovered after one round of self-calibration. For the bright pulsar B1822-14, self-calibration reduced the fitted size by $\sim 20\%$. We could therefore expect the scatter-broadening of our other target pulsars to be over-estimated by a similar factor, although the different observing conditions on each day could lead to variations.

4.8.2 Extrapolation of the measured pulse broadening

Locating scattering screens requires measurements of the angular and pulse broadening at the same frequency. In practice, the pulse broadening can only be measured at lower frequencies than the VLBA+VLA observations. As discussed in §4.1, we have extrapolated archival pulse broadening data to the observed frequencies. For sources with multiple measurements (J1746–2849, J1746–2856, B1758–23, B1822–14), the errors from extrapolation are likely less severe and can be estimated from the data. For J1745–2912

and B1809–176, only one measurement is available and so these errors could be larger. If we force $\alpha = 4$ as predicted for the thin screen model, all scattering locations move closer to Earth by $\approx 0.5 - 1$ kpc. In all cases except for B1822–14 and J1746–2856, this is within our 1σ uncertainty region. For the GC magnetar J1745–2900, $\alpha = 3.8 \pm 0.2$, while for B1822–14 $\alpha = 3.8 \pm 0.3$. Those values are consistent with either $\alpha = 4$ or 3.5. Measuring the temporal broadening more accurately would allow for a more robust inference of the scattering location.

4.8.3 Distance estimates

We have assumed that the GC pulsars are located at the GC distance of 8.3 kpc, as suggested by their high DM and τ values. The DM distance for B1758–23 is much larger than estimates from HI absorption and scattering (figure 9). For the other two sources, only DM distances are available. Those distances could therefore be subject to systematic error of up to $\approx 50\%$.

4.8.4 Possible effect on results

The phase calibration errors likely cause us to overestimate the angular broadening, θ . Extrapolation of the pulse broadening could cause us to underestimate τ for PSR J1745–2912 and B1809–176, if $\alpha < 4$. For the other sources, if the thin screen model holds and $\alpha = 4$, the τ values at high frequency could be overestimated. DM distances could be systematically off in either direction, but might be more likely to be overestimated (e.g. as for the GC pulsars and maybe B1758–23).

There are two relevant limits from equation (1), $\Delta/D \ll 1$ and $\Delta/D \approx 1$, for scattering local to and far from the source. In the former limit, $\Delta \sim D^2\theta^2/\tau$. In this case, overestimating D or θ has the same effect as underestimating τ : all of these errors would cause us to overestimate Δ . In the opposite limit, the dependence is most simply written as $D_s \sim \tau/\theta^2$. The distance to the scattering screen is roughly independent of source distance. Underestimating τ or overestimating θ would still mean that the screen is located closer to the source than we infer.

We simulate these effects using B1758–23 as an example, where $D_s = 2.0 \pm 0.5$ kpc using our best measurements. We choose this source because the adopted errors are relatively small, but it is low declination with evidence of phase calibration errors and has discrepant distance and τ measurements. If we were to use $\alpha = 4$, the extrapolated τ value could be $\approx 60\%$ smaller, larger than our adopted error bar. Then we would find $D_s = 1.5 \pm 0.4$ kpc. Repeating the exercise for a 20% smaller size or the larger DM distance, we find $D_s = 2.3 \pm 0.6$ kpc and $D_s = 2.7 \pm 0.8$ kpc. Each individual effect systemically shifts D_s at roughly the 1σ level.

Given the various possible systematic uncertainties, it is worth considering how the analysis presented here could be improved in the future. The low significance of our source detections leads to relatively poor size measurements. Higher signal-to-noise could allow phase self-calibration, reducing systematic calibrator errors as well as the statistical error bars on the sizes. Constraining image anisotropy would also allow us to test whether the same scattering medium

could be responsible for the images of both J1746–2849 and J1746–2856, for example. This could be achieved with longer integrations (all sources), by going to lower frequency where the pulsars are brighter (compact sources, although the phase calibrators may be heavily scatter-broadened), or by including the VLA in observations of non-GC pulsars. A better measurement of the frequency-dependence of the temporal broadening (α) might be even more important given the systematic uncertainties from extrapolation. This is also difficult for faint sources, especially at higher frequencies where the temporal broadening becomes much smaller than the intrinsic pulse width. We have also assumed a single, thin screen model in order to measure D_s . At low frequencies the shallow temporal broadening slopes $\alpha < 4$ imply that this assumption breaks down. At the higher frequencies of our VLBA+VLA observations the thin screen approximation may still be valid (Cordes & Lazio 2001). This assumption could be tested by measuring the frequency-dependence of both θ and τ , or for very bright sources through phase-resolved imaging. Both techniques have been used to show that the Sgr A* and GC magnetar images are likely dominated by a single thin screen (Bower et al. 2014; Spitler et al. 2014; Wucknitz 2015).

5 SUMMARY

We have used VLBA+VLA observations to measure the scatter-broadened image sizes of 6 of the most heavily scattered known pulsars. Combining the image sizes with previously measured temporal broadening of the pulse profiles leads to an estimate of the location of the scattering medium along the line of sight. A summary of our results follows.

- Three of the nearest pulsars to the GC magnetar SGR J1745–2900 have smaller image sizes despite comparable temporal scattering, evidence of additional strong scattering component closer to or even within the GC region. The strength of the Sgr A* / magnetar scattering screen decreases by at least a factor of 5 on scales of $\simeq 10$ pc. The GC region shows significant scatter-broadening on larger scales of $\simeq 100$ pc, which has contributions from at least two distinct sources (the screen responsible for the scattering of Sgr A* and SGR J1745–2900, Bower et al. 2014, and an additional screen $\lesssim 2$ kpc from the GC). The temporal broadening for all known GC pulsars is comparable $\simeq 1$ s at 1 GHz, $\lesssim 10^{2-3}$ orders of magnitude weaker than the proposed “hyperstrong” scattering medium in the GC. Nonetheless, the variable strength and locations of the scattering could imply variability in the temporal broadening with location and/or time, potentially reducing the sensitivity of past surveys to detecting short period (especially millisecond) pulsars.

- We tentatively measure a very compact size $\simeq 2$ mas for the GC pulsar J1745–2912. Combined with its large degree of temporal broadening, this measurement locates the scattering to $\lesssim 700$ pc of the source, likely within the GC region itself.

- The three non-GC pulsars in our sample all show scattering media located $\simeq 2$ kpc from Earth, likely within the Carina-Sagittarius spiral arm. In addition, all three have 3D positions consistent with known HII regions (S30, S40, S50, and in the case of B1758–23 also the supernova remnant W28).

• Assuming the likely association of the observed scattering with these HII regions, we calculate the minimum electron density required for them to produce the observed scattering. The corresponding minimum DM contribution is a large fraction $\gtrsim 25\%$ of the total, suggesting that distances to these pulsars, and others lying behind HII regions, based on their DM could be significantly over-estimated.

• Following Claussen et al. (2002), we independently constrain the distance to B1758–23 as $D = 5.3^{+1.4}_{-1.1}$ kpc based on its temporal and angular broadening and the angular broadening of a very nearby extragalactic background source. This distance agrees with both our revised distance estimate of $\simeq 6.1$ kpc from including the HII region DM contribution and a measurement from HI absorption of $D = 4 \pm 1$ kpc. It rules out an association of the pulsar with the supernova remnant W28.

• Finally, we have measured a new position of B1822–14, a known runaway pulsar (Moldón et al. 2012). Our added epoch further constrains the proper motion and confirms previous measurements of a space velocity $\simeq 750 \text{ km s}^{-1}$.

ACKNOWLEDGEMENTS

We thank the WISE team, Cordes & Lazio (2002), and Green (2014) for making their data publicly available and D.H.F.M. Schnitzeler for sharing ATCA position and flux density measurements for the GC pulsars studied here. JD was supported by a Sofja Kovalevskaja Award from the Alexander von Humboldt Foundation of Germany, and in part by the National Science Foundation under Grant No. NSF PHY-1125915. M. Kramer acknowledges financial support by the European Research Council for the ERC Synergy Grant BlackHoleCam under contract no. 610058. L.G.S. gratefully acknowledges support from the ERC Starting Grant BEACON under contract no. 279702 and the Max Planck Society. The Parkes radio telescope is part of the Australia Telescope, which is funded by the Commonwealth Government for operation as a National Facility managed by CSIRO. The National Radio Astronomy Observatory is a facility of the National Science Foundation operated under cooperative agreement by Associated Universities, Inc.

REFERENCES

- Anderson L. D., Bania T. M., Balser D. S., Cunningham V., Wenger T. V., Johnstone B. M., Armentrout W. P., 2014, *ApJS*, **212**, 1
- Arikawa Y., Tatsumatsu K., Sekimoto Y., Takahashi T., 1999, *PASJ*, **51**, L7
- Backer D. C., 1978, *ApJ*, **222**, L9
- Blandford R., Narayan R., 1985, *MNRAS*, **213**, 591
- Bower G. C., Backer D. C., Sramek R. A., 2001, *ApJ*, **558**, 127
- Bower G. C., Goss W. M., Falcke H., Backer D. C., Lithwick Y., 2006, *ApJ*, **648**, L127
- Bower G. C., et al., 2014, *ApJ*, **780**, L2
- Bower G. C., et al., 2015, *ApJ*, **798**, 120
- Britton M. C., Gwinn C. R., Ojeda M. J., 1998, *ApJ*, **501**, L101
- Chatzopoulos S., Gerhard O., Fritz T. K., Wegg C., Gillessen S., Pfuhl O., Eisenhauer F., 2015, *MNRAS*, **453**, 939
- Chennamangalam J., Lorimer D. R., 2014, *MNRAS*, **440**, L86
- Claussen M. J., Goss W. M., Desai K. M., Brogan C. L., 2002, *ApJ*, **580**, 909
- Cordes J. M., Lazio T. J. W., 1997, *ApJ*, **475**, 557
- Cordes J. M., Lazio T. J. W., 2001, *ApJ*, **549**, 997
- Cordes J. M., Lazio T. J. W., 2002, arXiv:astro-ph/0207156,
- Cordes J. M., Lazio T. J. W., 2003, ArXiv Astrophysics e-prints,
- Davies R. D., Walsh D., Booth R. S., 1976, *MNRAS*, **177**, 319
- Deneva J. S., Cordes J. M., Lazio T. J. W., 2009, *ApJ*, **702**, L177
- Dennison B., Thomas M., Booth R. S., Brown R. L., Broderick J. J., Condon J. J., 1984, *A&A*, **135**, 199
- Dexter J., O’Leary R. M., 2014, *ApJ*, **783**, L7
- Dexter J., et al., 2017, *MNRAS*, **468**, 1486
- Eatough R. P., et al., 2013, *Nature*, **501**, 391
- Foreman-Mackey D., Hogg D. W., Lang D., Goodman J., 2013, *PASP*, **125**, 306
- Frail D. A., Scharringhausen B. R., 1997, *ApJ*, **480**, 364
- Frail D. A., Diamond P. J., Cordes J. M., van Langevelde H. J., 1994, *ApJ*, **427**, L43
- Gillessen S., et al., 2017, *The Astrophysical Journal*, **837**, 30
- Goldreich P., Sridhar S., 2006, *ApJ*, **640**, L159
- Goodman J., Narayan R., 1985, *MNRAS*, **214**, 519
- Goss W. M., 1968, *ApJS*, **15**, 131
- Green D. A., 2014, *Bulletin of the Astronomical Society of India*, **42**, 47
- Greisen E. W., 2003, *Information Handling in Astronomy - Historical Vistas*, **285**, 109
- Gwinn C. R., Bartel N., Cordes J. M., 1993, *ApJ*, **410**, 673
- Hotan A. W., van Straten W., Manchester R. N., 2004, *Publ. Astron. Soc. Australia*, **21**, 302
- Ishimaru A., 1977, *Appl. Opt.*, **16**, 3190
- Johnston S., 1994, *MNRAS*, **268**, 595
- Johnston S., Koribalski B., Weisberg J. M., Wilson W., 1996, *MNRAS*, **279**, 661
- Johnston S., Kramer M., Lorimer D. R., Lyne A. G., McLaughlin M., Klein B., Manchester R. N., 2006, *MNRAS*, **373**, L6
- Kettenis M., van Langevelde H. J., Reynolds C., Cotton B., 2006, in Gabriel C., Arviset C., Ponz D., Enrique S., eds, *Astronomical Society of the Pacific Conference Series Vol. 351, Astronomical Data Analysis Software and Systems XV*. p. 497
- Lazio T. J. W., Cordes J. M., 1998, *ApJ*, **505**, 715
- Lazio T. J. W., Anantharamaiah K. R., Goss W. M., Kassim N. E., Cordes J. M., 1999, *ApJ*, **515**, 196
- Lewandowski W., Dembska M., Kijak J., Kowalińska M., 2013, *MNRAS*, **434**, 69
- Lewandowski W., Kowalińska M., Kijak J., 2015, *MNRAS*, **449**, 1570
- Little L. T., 1973, *Astrophys. Lett.*, **13**, 115
- Litvak M. M., 1971, *ApJ*, **170**, 71
- Lockman F. J., 1989, *ApJS*, **71**, 469
- Löhmer O., Kramer M., Mitra D., Lorimer D. R., Lyne A. G., 2001, *ApJ*, **562**, L157
- Lynds B. T., Oneil Jr. E. J., 1985, *ApJ*, **294**, 578
- Macquart J.-P., Kanekar N., Frail D. A., Ransom S. M., 2010, *ApJ*, **715**, 939
- Manchester R. N., Damico N., Tuohy I. R., 1985, *MNRAS*, **212**, 975
- Manchester R. N., Hobbs G. B., Teoh A., Hobbs M., 2005, *AJ*, **129**, 1993
- Moldón J., Ribó M., Paredes J. M., Brisken W., Dhawan V., Kramer M., Lyne A. G., Stappers B. W., 2012, *A&A*, **543**, A26
- Ng C., et al., 2015, *MNRAS*, **450**, 2922
- Psaltis D., Wex N., Kramer M., 2016, *ApJ*, **818**, 121
- Pynzar’ A. V., 2015, *Astronomy Reports*, **59**, 683
- Rajwade K., Lorimer D., Anderson L., 2016, preprint, (arXiv:1611.06977)
- Reid M. J., et al., 2014, *ApJ*, **783**, 130
- Sanna A., et al., 2014, *ApJ*, **781**, 108
- Schnitzeler D. H. F. M., Eatough R. P., Ferrière K., Kramer M., Lee K. J., Noutsos A., Shannon R. M., 2016, *MNRAS*, **459**, 3005

- Sharpless S., 1959, [ApJS](#), **4**, 257
- Shepherd M. C., Pearson T. J., Taylor G. B., 1994, in Bulletin of the American Astronomical Society. pp 987–989
- Sicheneder E., Dexter J., 2017, [MNRAS](#), **467**, 3642
- Spitler L. G., et al., 2014, [ApJ](#), **780**, L3
- Sternberg A., Hoffmann T. L., Pauldrach A. W. A., 2003, [ApJ](#), **599**, 1333
- Taylor J. H., Cordes J. M., 1993, [ApJ](#), **411**, 674
- Velázquez P. F., Dubner G. M., Goss W. M., Green A. J., 2002, [AJ](#), **124**, 2145
- Verbiest J. P. W., Weisberg J. M., Chael A. A., Lee K. J., Lorimer D. R., 2012, [ApJ](#), **755**, 39
- Wilkinson P. N., Narayan R., Spencer R. E., 1994, [MNRAS](#), **269**, 67
- Wucknitz O., 2015, preprint, ([arXiv:1501.04510](#))
- Yao J. M., Manchester R. N., Wang N., 2017, [ApJ](#), **835**, 29
- Yusef-Zadeh F., Goss W. M., Roberts D. A., Robinson B., Frail D. A., 1999, [ApJ](#), **527**, 172
- van Langevelde H. J., Frail D. A., Cordes J. M., Diamond P. J., 1992, [ApJ](#), **396**, 686
- van Straten W., Bailes M., 2011, [Publ. Astron. Soc. Australia](#), **28**, 1

This paper has been typeset from a $\text{\TeX}/\text{\LaTeX}$ file prepared by the author.